Eur. Phys. J. B **11**, 491–496 (1999)

THE EUROPEAN PHYSICAL JOURNAL B

EDP Sciences

Two-dimensional electron systems in inversion layers of p-type $Hg_{0.8}Zn_{0.2}Te$ metal-insulator-semiconductor structures

O. Rousière, D. Lemoine[a], H. Folliot, S. Hinooda, and R. Granger

Laboratoire de Physique des Solides, INSA, CS 14315, 35043 Rennes Cedex, France

Received 9 February 1999

Abstract. Strong oscillations on capacitance and conductance have been observed in p-type $Hg_{0.8}Zn_{0.2}Te$ metal-insulator-semiconductor structures, made by using a recent process for the interface passivation. This behaviour is attributed to a two-dimensional electron gas in the n-inversion layer and the variation of the conductance maximums with temperature indicates that the dominant perpendicular transport mechanism for electrons is an incoherent two-step tunnelling through deep levels in the gap. Three models have been used to describe the quantum confinement: the simple variational method, the triangular potential approximation and the propagation matrix method. The later approach takes into account the non parabolicity of the conduction band structure and uses a finite height barrier at the insulator-semiconductor interface. A very good agreement between experimental and calculated values for the two lowest subband energy is obtained.

PACS. 73.40.Qv Metal-insulator-semiconductor structures (including semiconductor-to-insulator) – 81.40.Rs Electrical and magnetic properties (related to treatment conditions) – 73.20.Dx Electron states in low-dimensional structures (superlattices, quantum well structures and multilayers)

1 Introduction

Quantization of energy levels in semiconductor inversion layers has been studied since many years and its investigation constitutes always a important domain for the fundamental research. For bound states in surface layers on narrow gap semiconductors, there is a strong coupling between the conduction and the valence bands with, as a consequence, a nonparabolic conduction band with a small effective mass of electrons at its bottom. The usual one-band approximation is even less suitable to describe the corresponding states than the band gap is small.

$Hg_{1-x}Zn_xTe$ is a pseudobinary semiconductor which shows a direct bandgap adjustable through composition x. This compound is potentially usable for the infrared detection as well as HgCdTe which has a weaker structural stability. The performances of infrared devices are very sensitive to their surface passivation and interfacial properties often limit the detector efficiency. A recent passivation process [1] enables to obtain HgZnTe with high quality surfaces. The minimum of the interface state density is close to 10^{10} eV^{-1} cm^{-2} and its energy distribution displays a broad U-shape with a small increase near band edges. This surface treatment allows us to investigate the behaviour of the two-dimensional (2D) electron gas built in the n-type inversion layer of a metal-insulator-semiconductor (MIS) structure elaborated on p-type $Hg_{0.8}Zn_{0.2}Te$. Our experiments are carried out by measuring capacitance C and conductance G as a function of the inversion polarisation V, frequency ω and temperature T.

Strong oscillations on $C(V)$ and $G(V)$ curves are observed, which are induced by the surface quantization under certain conditions. Similar features have been already reported for HgCdTe [2–7] but, to our knowledge, it is the first time that the response of 2D electron gas generated in an inversion layer is observed on a HgZnTe surface. From the temperature dependence of conductance maximums, an incoherent two-step tunnelling through deep levels in the gap has been recognized as the dominant perpendicular transport mechanism for electrons between valence band states and the two-dimensional subbands. The detailed analysis of experimental data is made by comparison of subband energy values obtained from the variational method, the triangular potential approximation and the propagation method. The accuracy of the last method has been estimated by comparison with the results of numerical self-consistent calculations of the bound states with a height-band Hamiltonian [8].

2 Experimental

p-$Hg_{0.8}Zn_{0.2}Te$ slices are cut from an ingot grown by a two step method. First, the travelling heater method (THM) [9] is used for the ingot growth. It is followed by a solid state recrystallization without intentional doping.

[a] e-mail: daniel.lemoine@insa-rennes.fr

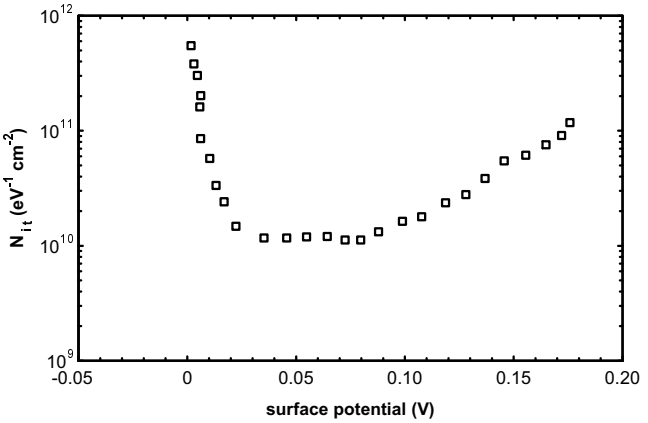

Fig. 1. Distribution of the interface state density $N_{\rm it}$ as a function of the surface potential. The results are obtained from $C(V)$ data analyzed according to the Terman method for an interface passivated and prepared as specified in the text.

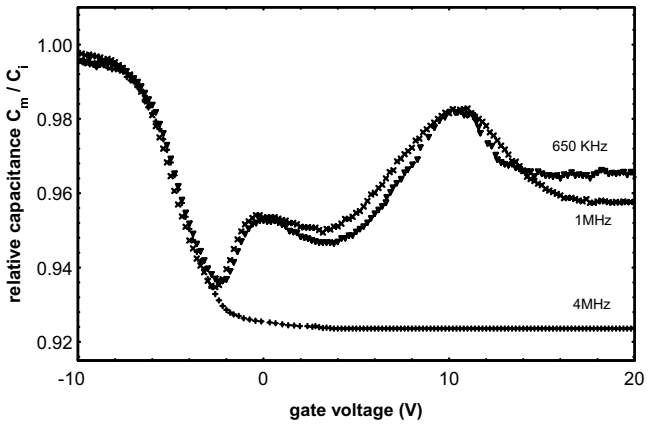

Fig. 2. Typical capacitance $C_{\rm m}/C_{\rm i}$ obtained at 77 K for three measurement frequencies *versus* gate voltage.

So obtained samples show a very low variation of composition x. Wafers are then annealed at 400 °C under a Hg overpressure to remove as far as possible tellurium precipitates and to reduce the Hg vacancy concentration. However they remain p-type. After the mechanical polishing of the surface which is ended with 0.02 μm alumina powder and degreasing, a first etching of the sample is done in a 1% by volume bromine solution in methanol. The wafers are rinsed in de-ionised (DI) water and then dipped in a 0.1% Br_2-methanol solution. A long rinsing in DI water precedes the passivation process. The sample is finally dipped 30 seconds in a solution of 0.1% Br_2-methanol to which is added 0.02% by volume of 1M $Na_2S \cdot 9H_2O$ in ethylene glycol [1]. The treatment ends with a long rinsing in DI water followed by a drying under a nitrogen flux. The whole of this process is performed at room temperature. After this preparation, the surface topography, as monitored by atomic force microscopy, shows a very small roughness which root mean square amplitude is 0.3 nm [1].

This surface is then covered with a dielectric layer of SiO of several hundreds of nanometers evaporated with an e-beam gun at a slow rate ($\sim$ 3 to 6 nm/min) under ultra high vacuum. Indium gates are deposited through a metal mask to complete MIS structures. An HP 4192A Impedance analyser and an EGG 5210 lock-in amplifier are used for C and G measurements depending on the frequency while $C(V)$ characteristics at 1 MHz are monitored with an HP 4280A C-meter. Each sample is put in a cryostat inside an isothermal cell and in the dark during the measurements. Before admittance measurements, a negative bias is applied to the MIS device which is progressively increased during several hours at room temperature. The electric field at the interface entails a great number of deep traps to be charged positively. The sample is next cooled down at the measurement temperature. The flatband voltage is so shifted towards negative voltages and the electric field in the insulator is reduced when the applied bias places the MIS structure in strong inversion. This procedure allows us to investigate MIS samples up to more positive gate biases before the breakdown in the insulator. This sample preparation do not alter the energy distribution of fast interface states which is shown in Figure 1, as deduced from the Terman analysis [10] at 77 K.

3 Results and discussion

Under inversion bias, both $C_{\rm m}(V)$ and $G_{\rm m}(V)$ experimental curves show pronounced oscillations when the measurement frequency is intermediate (between 50 kHz and 2 MHz at $T = 77$ K depending on samples). The position of capacitance oscillations is independent of the frequency in the frequency range where they are observed. A capacitance maximum occurs for a gate voltage corresponding to the coincidence of the Fermi level at the surface with a subband energy level, which appears broadened by temperature effects and also by the non uniform distribution of interface charges. Figure 2 shows typical $C_{\rm m}(V)$ curves obtained at $T = 77$ K for three frequencies: two capacitance oscillations are well revealed at 650 kHz and 1 MHz in strong inversion while the capacitance shows no variation in the same bias range at 4 MHz (high frequency behaviour). In this latter case, the supply of electrons to 2D energy levels has a response time much longer than the period of the applied signal. Oscillations disappear also when the frequency decreases and $C_{\rm m}(V)$ curves have then the classical low frequency feature. This behaviour is explained by the increasing number of interface states that are able to follow the small-signal voltage at decreasing frequencies. Their contribution masks the capacitance response of the 2D electrons. It is necessary to correct $G_{\rm m}$ data from the serial resistance $R_{\rm s}$ and the insulator capacitance $C_{\rm i}$ to obtain the parallel conductance $G_{\rm p}$, as shown in the equivalent circuit of the MIS structure (Fig. 3). After this correction, $G_{\rm p}(V)$ oscillations coincide with those of $C_{\rm p}(V)$ and Figure 4 shows capacitance $C_{\rm p}(V)$ and conductance $G_{\rm p}(V)$ obtained at 1 MHz and at $T = 77$ K for sample B. The variation with temperature of the parallel conductance $G_{\rm p}$ measured at 1 MHz is reported in Figure 5 for two gate voltages corresponding to oscillation maxima. $\ln(G_{\rm p})$ increases with temperature T up to 90 K and next decreases. This behaviour has often been

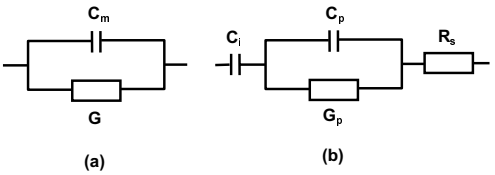

Fig. 3. Equivalent circuit for a MIS structure: (a) $C_{\rm m}$ and $G_{\rm m}$ are the measured electrical components for the MIS sample, (b) $C_{\rm p}$ and $G_{\rm p}$ are the parameters relative to the semiconductor part.

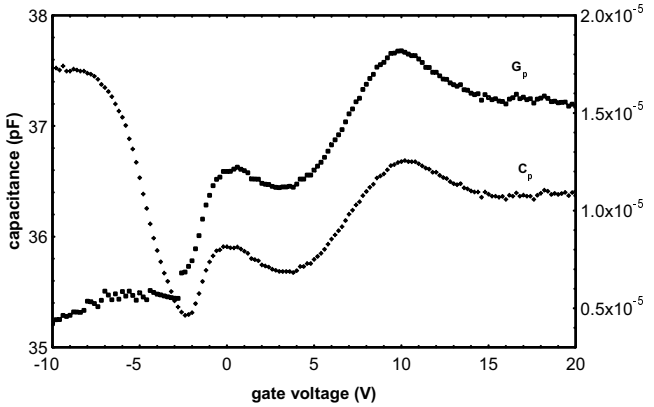

Fig. 4. Capacitance $C_{\rm p}$ and conductance $G_{\rm p}$ as a function of gate voltage at 1 MHz and 77 K (sample B).

observed in p-HgCdTe MIS structures [3,4]. It is interpreted by considering an incoherent two-step tunnelling process as the dominant transport mechanism. For this two-step trap-assisted model, electrons first tunnel from the valence band into deep traps and then tunnel toward the 2D inversion layer, as recalled in Figure 6, where both successive steps 1 and 3 are shown. While tunnelling process cannot directly account for the observed temperature dependence, Yang *et al.* [3,4] have shown, in the high temperature side, that the positive band gap temperature coefficient $\mathrm{d}E_{\rm g}/\mathrm{d}T$ for HgCdTe leads to a conductance decrease when the temperature is raised. For HgZnTe, the energy gap $E_{\rm g}$ is obtained using the expression of Toulouse *et al.* [11]:

$$E_{\rm g}(x,T) = -0.3 + 3.24\times10^{-2}x^{1/2} + 2.731x - 0.629x^2 + 0.533x^3 + 5.3\times10^{-4}T \times (1 - 0.76x^{1/2} - 1.29x)$$

and $\mathrm{d}E_{\rm g}/\mathrm{d}T = 2.131\times10^{-4}\,\mathrm{eV\,K^{-1}}$ for $x = 0.2$. Assuming a triangular potential barrier, the tunnelling probability $P_{\rm t}$ between deep states and the 2D level is proportional to [12]

$$\exp\left[-8\pi\sqrt{2m^*}\,(\eta E_{\rm g})^{3/2}\,\Big/3e\hbar F\right]$$

where F is the electric field, m^* the effective electron mass, e the elementary charge and h the Planck constant ($\hbar = h/2\pi$). η is a coefficient between 0 and 1 depending on the energy position of the deep level. The bandgap has so a strong effect on the tunnelling probability $P_{\rm t}$ and

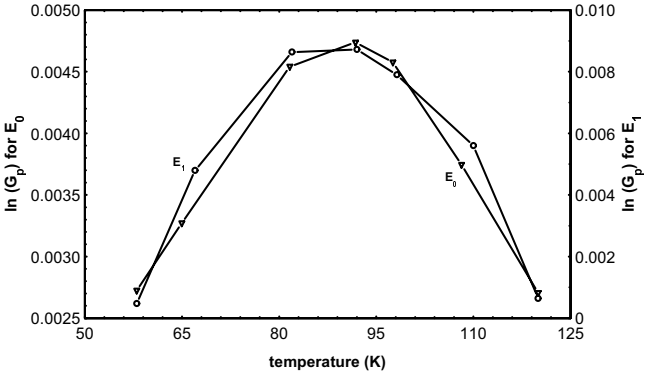

Fig. 5. Plots of conductance maximums (in semilogarithmic scale) for the two lowest subband energies (labelled E_0 and E_1) *versus* temperature.

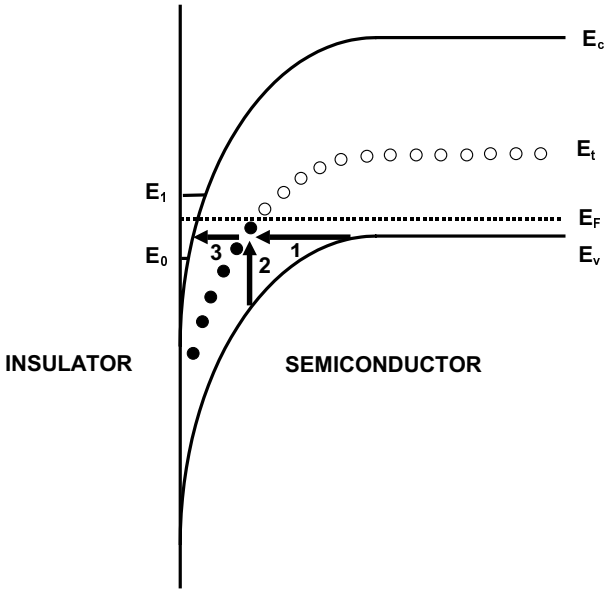

Fig. 6. Band bending diagram in strong inversion conditions. Arrows labelled 1, 2 and 3 show the various possible transitions for electrons.

its temperature variation involves a conductance decrease when the temperature is raised. Zvara *et al.* [13] and Lang *et al.* [7] have observed the same behaviour at low temperature on p-type HgCdTe whereas Waterman *et al.* [5] have recognized a trap assisted tunnelling process with a first thermally induced transition of an electron from the valence band to a deep level in the band gap (steps 2 and 3 in Fig. 6).

In order to check the evolution of MIS structure characteristics with time, several samples have been kept for 4 months either under vacuum or at the ambient atmosphere. Admittance measurements have shown that electrical characteristics are very little changed after sample conservation under vacuum and the capacitance and conductance oscillations are always observed. For samples left at the ambient atmosphere, no oscillation appears in strong inversion on the experimental curves whatever the used frequency. The Terman analysis of $C(V)$ curve in the depletion region shows a general increase of the energy

Table 1. Sample characteristics and results of calculations using three different models.

sample	A	B	C	D
from experimental data				
N_a-N_d (cm^{-3})	7.8×10^{15}	9.0×10^{15}	8.0×10^{15}	1.0×10^{16}
N_{dep} (cm^{-2})	6.2×10^{11}	6.2×10^{11}	6.3×10^{11}	7.9×10^{11}
E_0 (meV)	95	103	110	138
E_1 (meV)	160	186	211	255
variational method				
E_0 (meV)	85	93	104	128
$\langle V_i \rangle$ (meV)	3.7	3.8	3.9	4.1
z_{av0} (nm)	11.1	10.4	10.1	9.7
triangular potential approximation				
E_0 (meV)	86	95	105	130
z_{av0} (nm)	10.3	9.7	9.5	8.9
E_1 (meV)	155	181	203	245
propagation matrix method				
E_0 (meV)	90	96	112	141
m^*_0 / m_0	0.0191	0.0196	0.021	0.023
z_{av0} (nm)	7.9	7.1	6.5	6.0
E_1 (meV)	163	184	206	263
m^*_1 / m_0	0.0255	0.027	0.029	0.034

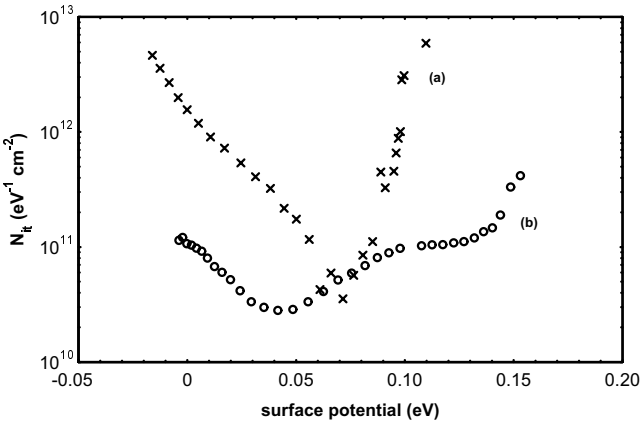

Fig. 7. Distribution of the interface state density N_{it} as a function of surface potential after a sample conservation of 4 months: (a) at the ambient atmosphere, (b) under vacuum.

distribution of fast interface states (see Fig. 7). Fluctuations of the interface charge density yield a wide smearing out of the subband edges, which doesn't allow to see any oscillation.

In the inversion region, the potential energy $V(z)$ is the sum of three contributions resulting from the presence of depletion and inversion charges and of image charges due to the high permittivity discontinuity at the insulator-semiconductor interface. The corresponding potentials have been described in the Hartree approximation by Stern [14] and Ando *et al.* [15]. Three approaches have been used and compared to describe the bound states and the wave functions in n-inversion layers on p-$Hg_{1-x}Zn_xTe$.

(i) The variational method: we have used the trial eigenfunction with a single parameter b for the lowest subband [16]:

$$\zeta_0(z) = \left(b^3/2\right)^{1/2} z \exp(-bz/2).$$

The minimization on the energy of the level is performed numerically as the image potential $\langle V_i \rangle$ is taken into account. Results for four samples are given in Table 1 for the lowest subband with the average distance of the charge z_{av}. For the second subband, this method gets more complicated and has not been used.

(ii) The triangular potential approximation: neglecting the image potential, the energy shows a quasi linear increase very near the insulator-semiconductor interface. Airy functions are solutions of the Schrödinger equation under the assumption of constant effective

mass and the eigenvalues E_i have been calculated accurately for the lowest subbands [17]. This method can be a good approximation when the depletion region is much wider than the inversion layer, which is the usual case and the one for the samples studied.

(iii) The propagation method: the Schrödinger equation is solved in a one-dimensional potential well with an arbitrary shape. The well is divided into N parts of length Δz_n so that the potential can be considered constant within Δz_n. The continuity of the wave function $\Psi(z)$ and of $\frac{1}{m(z)}\frac{d\Psi(z)}{dz}$ at each region boundary lead to the eigenenergy values of the potential well [18,19]. The nonparabolicity of the conduction band is taken into account using a two-band $k \times p$ model for each Δz_n interval. Moreover, a barrier of a finite height (~ 4.1 eV) is placed at the insulator-semiconductor interface.

The whole of the results is gathered in Table 1. N_a-N_d is obtained from the analysis of $C(V)$ curves in the depletion region, according to a numerical procedure which takes into account the special features of narrow band gap semiconductors [20]. N_{dep} is the total number of charges in the inversion layer. The uncertainty on the subband energy levels obtained from $C_m(V)$ data is estimated to be about 5 meV. The effective mass values obtained from the propagation method, have been used for the variational calculation and for the triangular approximation to determine the subband energies. Results from the propagation method are the closest of the ones obtained from experimental data, particularly for the second subband. For the lowest subband, the variational method and the triangular potential approximation give results very near to each other but are always slightly lower than experimental values. Since it was predictable, subband energies increase with increasing of the total space charge and especially of the total number of charges N_s in the inversion layer, which raises the average electric field near the insulator-semiconductor interface. Nachev has performed the most detailed analysis of the 2 D electronic states [8]: self-consistent calculations are solved in the Hartree approximation on the basis of a eight-band Hamiltonian, *i.e.* taking into account the conduction band, the heavy-hole, light-hole and split-off valence bands for both spin directions. Only the effect of the image potential is neglected. In order to estimate the error due to the approximations of the propagation method, we have performed the calculations in the case of a HgCdTe sample investigated in the work of Nachev. For $Hg_{0.8}Cd_{0.2}Te$ (with an energy gap $E_g = 58.3$ meV), the energy level of the first and second subbands, as calculated for $N_a = 5 \times 10^{16}$ cm^{-3} and $N_s = 3 \times 10^{11}$ cm^{-2}, are $E_0 = 121$ meV and $E_1 = 169$ meV. With the same parameters and calculation conditions, the propagation method gives $E_0 = 126$ meV and $E_1 = 170$ meV. Results are close enough in this case and the propagation method must be more a better approximation for HgZnTe samples studied, as they have a higher band gap ($E_g = 256$ meV) and therefore, show a smaller interaction between bands. The result of a self-consistent calculation depends strongly on the applied boundary conditions. When the charge density in the semiconductor increases (with N_{dep} and N_s), the potential of the inversion layer is steeper and the interfacial confinement raises. As a result, the electron wave function must begin to penetrate the heterojunction barrier, which leads first, to a lower subband energy and secondly, to a smaller average distance z_{av} as compared to the corresponding values calculated with a infinite barrier, as considered in the work of Nachev. Figure 8 shows the wave functions $\psi_0(z)$ and $\psi_1(z)$ for the two lowest subbands of sample A obtained from the propagation method. It appears that the electron envelope function vanishes not abruptly at the interface but extends into the insulator on more than one nanometer. As a consequence, the average penetration value z_{av} (see in Tab. 1) obtained from the propagation method is clearly lower than the ones calculated from the other approaches by taking an infinite barrier at the interface. The relative difference on z_{av} is higher than 30% for the states of the lowest subband.

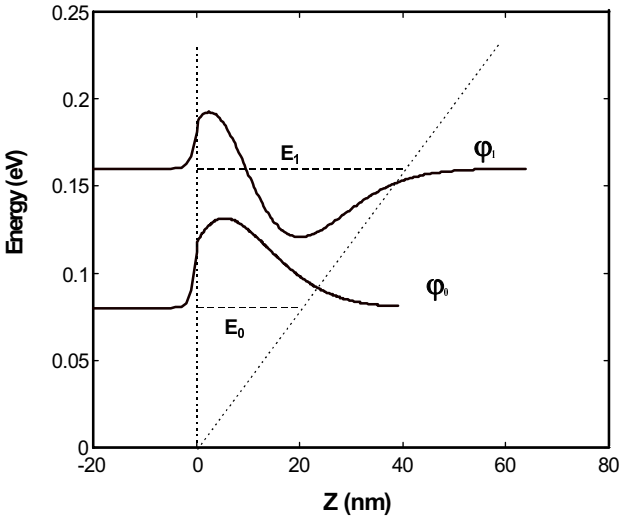

Fig. 8. Wave functions $\psi_0(z)$ and $\psi_1(z)$ for the two lowest subbands in the n-inversion layer calculated with the propagation matrix method as a function of the distance from the interface (sample A).

The first subband energies obtained from the variational method and the triangular potential approximation are close among them but lower of about 10% than experimental values, which is little considering all of approximations used. The agreement of our calculation of energy levels from the propagation method is good for the whole of the samples studied. The results remain all in the limit of the experimental uncertainty. This agreement seems however to be the best in the case of the higher negative charge densities in the semiconductor, *i.e.* when the Hartree approximation is the most justified (example of sample D). If the electron density in the inversion layer is small, the exchange and correlation effects are partially cancelled by the ones due to the image potential [15]. These two effects have been neglected in our calculations.

4 Summary

A recent passivation process enables us to obtain HgZnTe surfaces of high quality. So, strong oscillations on $C_{\mathrm{m}}(V)$ and $G_{\mathrm{m}}(V)$ have been observed for the first time on HgZnTe MIS samples and show the existence of a two-dimensional electron gas at the interface. The variation of the conductance maximums with temperature indicates that the dominant perpendicular transport mechanism for electrons is an incoherent two-step tunnelling *via* deep levels in the gap.

Three approaches have been used to obtain subband energy levels. The simple variational method and the triangular potential approximation lead to energies which are close for the lowest subband, but anyway lower than experimental values. With the propagation method, we take into account the non parabolicity of the conduction band structure by considering a variation of the effective mass from the two-band $k \times p$ model. Moreover, the insulator-semiconductor interface is described with a barrier of finite height. Results obtained in a self-consistent way with this method are in good agreement with those calculated by Nachev [8], who has solved the problem in the Hartree approximation on the basis of a eight-band Hamiltonian. For the whole of our samples, the energy of the levels obtained from the propagation method for the two lowest subbands is very close to what is experimentally observed, which confirms the validity of this approach in the case of HgZnTe with a small band-gap.

The authors would like to thank R. Triboulet (CNRS Meudon, France) for providing the HgZnTe ingot. We also acknowledge J.C. Chabreyron for his technical assistance.

References

1. O. Rousière, D. Lemoine, A. Quémerais, C.K. Assi, R. Granger, R. Triboulet, Semicond. Sci. Technol. **13**, 622 (1998).
2. J.D. Beck, M.A. Kinch, E.J. Esposito, R.A. Chapman, J. Vac. Sci. Technol. **21**, 172 (1982).
3. C.H. Yang, M.J. Yang, J.D. Beck, Phys. Rev. B **38**, 12760 (1988).
4. C.H. Yang, M.J. Yang, J.D. Beck, Semicond. Sci. Technol. **5**, S118 (1990).
5. J.R. Waterman, R.J. Wagner, J.M. Perez, J. Vac. Sci. Technol. A **7**, 381 (1989).
6. R. Sizmann, J. Chu, F. Koch, J. Ziegler, M. Maier, Semicond. Sci. Technol. **5**, S111 (1990).
7. M. Lang, J. Humenberger, K.H. Gresslehner, K. Lischka, J. Crystal Growth **117**, 954 (1992).
8. I. Nachev, Semicond. Sci. Technol. **3**, 29 (1988).
9. R. Triboulet, A. Lasbley, B. Toulouse, R. Granger, J. Crystal Growth **79**, 695 (1986).
10. L.M. Terman, Solid-State Electron. **5**, 285 (1962).
11. B. Toulouse, R. Granger, S. Rolland, R. Triboulet, J. Physique **48**, 247 (1987).
12. A. Rogalski, J. Piotrowski, Prog. Quantum Electron. **12**, 87 (1989).
13. M. Zvara, R. Grill, P. Hlidek, P. Höschl, M. Lang, K. Lischka, Semicond. Sci. Technol. **11**, 1718 (1996).
14. F. Stern, Phys. Rev. B **5**, 4891 (1972).
15. T. Ando, A.B. Fowler, F. Stern, Rev. Mod. Phys. **54**, 437 (1982).
16. F.F. Fang, W.E. Howard, Phys. Rev. Lett. **16**, 797 (1966).
17. M. Abramowitz, I.A. Stegun, *Handbook of Mathematical Functions* (U.S. GPO, Washington, 1964).
18. E. Merzbacher, *Quantum Mechanics* (Wiley, New York, 1970).
19. S.L. Chuang, *Physics of Optoelectronic Devices* (Wiley, New York, 1995).
20. O. Rousière, D. Lemoine, A. Quémerais, R. Granger, S. Rolland, R. Triboulet, J. Vac. Sci. Technol. A **16**, 2300 (1998).